HiSST: 2nd International Conference on
High-Speed Vehicle Science & Technology
11–15 September 2022, Bruges, Belgium

Experimental Investigation of Transpiration Cooling in a Subscale Combustion Chamber with Non-Reactive Flow

Jonas Peichl[1], Andreas Schwab[2], Markus Selzer[1], Hannah Böhrk[1,3], Jens von Wolfersdorf[2]

Abstract

This paper presents the first results of a study of transpiration cooling in a segmented ceramic matrix composite specimen resembling a subscale rocket engine combustion chamber. The tests were conducted with a hot air mainstream flow with a temperature of T_{hg} = 800 K, and cold air as coolant. For the first experiments, a variation of the blowing ratio of F = 0-0.75% was investigated, with constant blowing over all segments. The increase of cooling efficiency with rising blowing ratio is demonstrated. For the nozzle contoured segment, a significant increase of the wall temperature could be determined for low blowing ratios, which can be attributed to cross-flows caused by the higher pressure gradient in the expansion section.

Keywords: *Transpiration cooling, rocket engine combustion chambers, ceramic matrix composites*

Nomenclature

Latin

a – thermal diffusivity
A – area
d – diameter
F – blowing ratio
k – thermal conductivity
K_D – Darcy coefficient
K_D – Forchheimer coefficient
L – length
$\dot{m}$ – mass flow rate
M – Mach number
P, p – pressure
Re – Reynolds number
T – Temperature
u – velocity
x, y – rectagular coordinates

Greek

ρ – density
μ – viscosity
ϵ – area ratio

Subscripts

cg – cold gas
hg – hot gas
con – contraction
exp – expansion
i – inner
in – inlet
o – outer
out – outlet
hg – hot gas
tot – stagnation state
0 – without blowing
max – maximum
$\perp$ – Orthogonal to fiber direction
$\parallel$ – Parallel to fiber direction

1. Introduction

High demands are placed on the combustion chambers of chemical propulsion systems for future space transportation systems. Increasing thermal and mechanical loads due to increasing combustion chamber pressures and the demand for increased structural life time for reusable launch vehicles are driving factors for the current development. With wall heat fluxes in the nozzle throat region reaching over

[1] *Institute for Structures and Design, German Aerospace Center (DLR), Pfaffenwaldring 38-40, 70569 Stuttgart, Germany, Jonas.Peichl@dlr.de*
[2] *Institute for Aerospace Thermodynamics; University of Stuttgart, Pfaffenwaldring 31, 70659 Stuttgart Germany*
[3] *Now at DHBW Stuttgart*

80 MW/m^2 for the European Vulcain rocket engine [1], an effective cooling system is required for the combustion chamber to endure the severe thermal loads. Herefore, transpiration cooling as a highly efficient cooling method could be used as a disruptive approach. The principle of transpiration

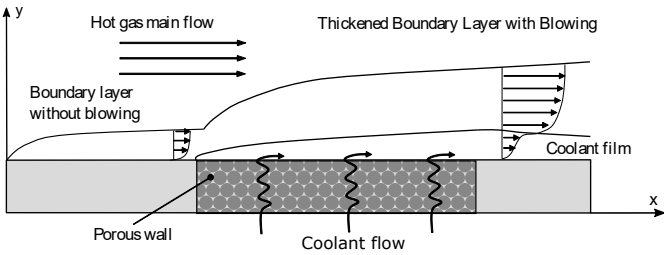

Fig 1. Schematic description of transpiration cooling[5]

cooling is shown schematically in Fig 1. A coolant is forced through a porous structure, creating an internal cooling effect by exchanging heat with the solid structure. Furthermore, the coolant exiting the porous wall forms a protective cooling film between the hot gas main flow and the porous wall, decreasing the incoming heat flux into the wall. Although showing high cooling effectiveness compared to regenerative and film cooling as shown e.g. by Eckert and Livingood [2], transpiration cooling has only found application in thermally relatively low loaded structures, as e.g. in the injector head of the Space Shuttle Main Engine [3]. A major challenge in applying transpiration cooling on thermally high loaded structures is the manufacturing of a suitable permeable material. At the Institute of Structures and Design of the German Aerospace Center, transpiration cooled combustion chambers are being developed using porous high temperature ceramic matrix composite materials. The goal is to significantly increasing combustion chamber life time and thus enabling reusable rocket engines, furthermore to decrease engine mass and manufacturing cost.

In order to develop enhanced tools and methods for the design of transpiration cooled hot structures, fundamental studies of the transpired coolant boundary layer development and the thermal response of the porous material have to be conducted. These experiments are being performed in a cooperation between the DLR Institute for Structures and Design and the Institute for Aerospace Thermodynamics of the University of Stuttgart. Previous studies focused on the investigation of material-internal heat transfer and fluid-fluid boundary layer interactions with a single planar sample as described in Langener et al. [4] and Schweikert [5]. In order to further optimize the already high cooling efficiency, the cooling effect could be tailored to the apparent heat loads by locally controlling the coolant mass flow. The experimental setup of Schweikert was therefore extended to four planar transpiration cooled samples exposed to moderate temperature hot air flows, as described in Schwab et al. [6] and Peichl et al. [7].

To ”fill the gap” between the extensive fundamental investigations and more application-oriented tests of subscale combustion chambers under realistic conditions comparable to e.g. Ortelt et al. [8], the following experimental study was devised. The transpiration cooling specimen resembles a scaled-down rocket engine combustion chamber which is tested under elevated thermal loads and non-reactive hot air flow. This setup improves the degree of realism compared to the fundamental experiments, but neglects effects like thermal transients, foreign gas injections and chemical reactions which would be apparent in combustion chamber tests.

2. Experimental Setup

The described experimental study was conducted at the High Temperature Facility (HTF) at the Institute for Aerospace Thermodynamics (ITLR) of the University of Stuttgart. In the following, a brief description of the HTF is given. Furthermore, the design and characterization of the segmented transpiration cooling specimen is described.

2.1. High Temperature Facility

The HTF facility is a hot gas wind tunnel which was initially designed for conducting research on combustion under supersonic flow conditions [9]. A schematic depiction of the test rig can be found in Fig. 2 The hot gas main flow is fed to the test facility via an electrically driven screw compressor, providing

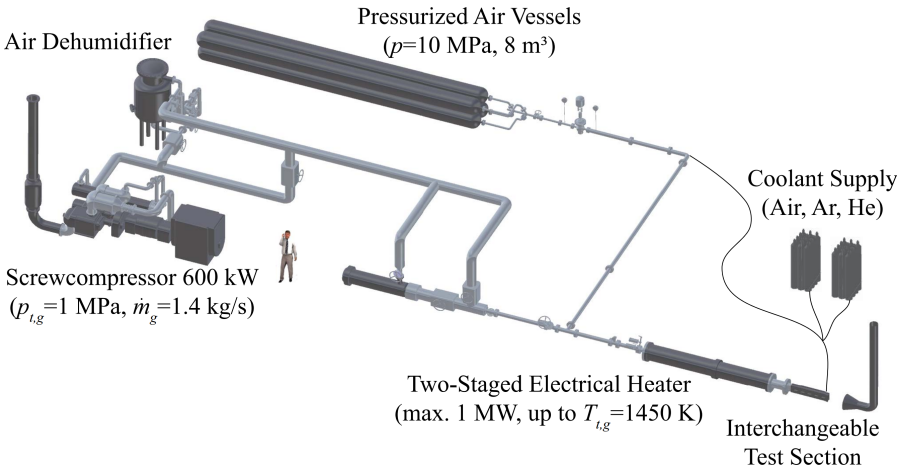

Fig 2. High Temperature Facility at ITLR [4]

mass flow rates of $\dot{m}_{hg,max}$= 1.4 kg/s at pressures of $p_{0,max}$ = 1 MPa. The compressed air is being dehumidified by a pebble bed dryer, resulting in a residual relative air humidity of 0.1%. The air flow is then heated convectively by a two staged electrical heater with a maximum power supply of 1 MW, allowing maximum total temperatures of up to $T_{0,max}$ = 1450 K. In a enclosing plenum, the resulting hot gas conditions are measured using a Keller PAA22-C-10 pressure sensor (p = 0-10 bar, $\pm$ 0.5% FS) and four thermocouples. The resulting volume flow is measured with a Endress+Hauser Prowhirl 77H. A flange connection allows the attachment of the test specimen, which is depicted in Fig. 3. For cooling experiments, the cooling air flow is supplied by multiple pressurized air vessels.

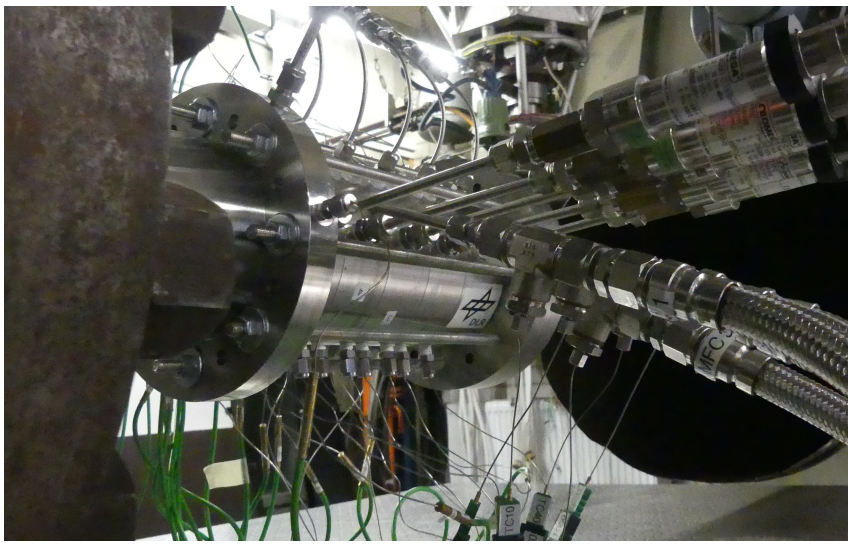

Fig 3. Transpiration cooling experiment integrated at High Temperature Facility

2.2. Transpiration cooling Specimen

2.2.1. General setup

The serial transpiration cooling specimen is shown in Fig. 4. A stainless steel inlet nozzle adapts the outlet diameter of the HTF plenum to the inner main stream flow diameter of the transpiration cooling specimen. The test specimen consists of a segmented stack with five segments which can be indepen-

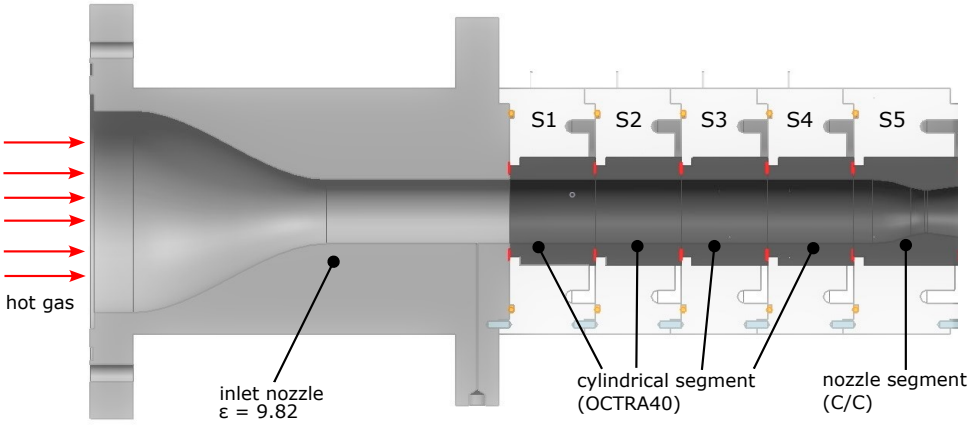

Fig 4. Crossection of transpiration cooling specimen

dently fed with a defined coolant mass flow rate. The specimen geometry resembles a sub-scale rocket engine combustion chamber, with four segments having a cylindrical inner geometry (S1-S4), as well as one segment having a Laval type convergent-divergent nozzle cross section (S5).

Figure 5 exemplary shows the layout of a single segment of the stacked specimen. In the center of the segment, the permeable liner is located, which is made of a porous ceramic matrix composite (CMC) material. The material choice for the respective segments is discussed in section 2.2.2.

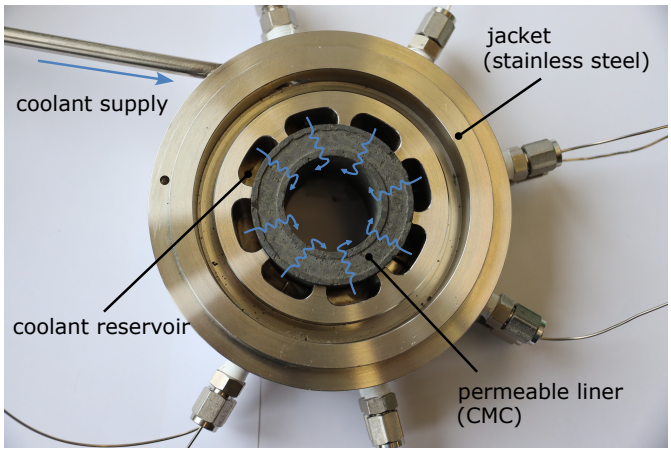

Fig 5. Cylindrical Segment

Each liner segment is equipped with four type-K thermocouples (accuracy $\pm$ 1.5 K). The thermocouples are placed radially 7 mm downstream of the beginning of the segment and are distributed on both the hot gas side liner surface as well as in the liner bulk material for the determination of the wall internal

temperature distribution. To attain a proper adhesive contact to the solid bulk material even at high wall temperatures of $T_{w,max}$ = 800 K, the thermocouples are bonded with Graphi-Bond 669 graphite adhesive.

The pressures on the inner wall of the liner are measured at the same axial position, using a DSA3016 pressure transducer (fullscale range 700 kPa, accuracy $\pm$ 0.05% FS) acquired via a DSAENCL 3200 enclosure. The liner is encased by a jacket made of stainless steel, with milled groove structures acting as a coolant reservoir on the backside of the liner. The coolant mass flow rate fed to the cylindrical segments 1, 2 and 4 is controlled by a Wagner/Bronkhorst F-203AV-M50-RDG-55-V allowing mass flow rates of $\dot{m}_c$ = 0-10.75 g/s ($\pm$0.5% RD plus $\pm$0.1% FS) as well as a Teledyne-Hastings HFC-303 ($\dot{m}_c$ = 0-10.75 g/s $\pm$ 0.1 g/s) for segment S3. For the nozzle segment S5, due to the larger outlet area, higher mass flow rates are required, hence a Bronkhorst/Wagner F-203AV-1M0-RGD-55-V mass flow controller is deployed, allowing mass flow rates of 21.5 g/s ($\pm$ 0.5% RD plus $\pm$0.1% FS).

The temperature of the coolant supply and inside the coolant reservoir are measured with type-K thermocouples (accuracy $\pm$ 1.5 K) The pressure inside the coolant reservoir is measured using Newport Omega PAA33X-C-15 pressure sensors (p = 0-15 bar, $\pm$ 15 mbar).

The parameters for the cylindrical section were chosen based on previous studies [10] on transpiration cooled CMC combustion chambers by the Institute of Structures and Design. The scale-down of the geometry was based on heat flux scaling techniques for combustion devices as proposed by Dexter et al. [11] The segments are separated by a 5 mm thick bulkhead on the reservoir side, located at the upstream side. The porous liners are sealed against the other segment liners using SIGRAFLEX carbon seals. The geometric parameters of the liner segments are given in Tab. 1 and Tab. 2. The nozzle

Table 1. Segment geometry cylindrical

Parameter	Symbol	Unit	Value
Inner diameter	d_i	mm	30
Outer diameter	d_o	mm	50
Segment length	L	mm	40
Effective segment length	L_{eff}	mm	35

contraction ratio $\epsilon_{con} = A_i/A_{th}$ was chosen to represent a typical rocket engine combustion chamber. The nozzle was designed to have an expansion flow adapted to the ambient pressure, hence preventing shock wave formation and flow separation inside the nozzle. This is achieved with an expansion ratio $\epsilon_{exp} = A_{out}/A_{th}$ of 1.48. As no permeation is possible through the bulkhead, a 5 mm portion at the upstream side of the porous segment is impermeable, reducing the total segment length L to the effective segment length L_{eff} which is perfused.

Table 2. Segment geometry nozzle

Parameter	Symbol	Unit	Value
Inner diameter	d_i	mm	30
Throat diameter	d_{th}	mm	20
Outer diameter	d_o	mm	50
Segment length	L	mm	50
Effective segment length	L_{eff}	mm	45
Contraction ratio	ϵ_{con}	-	2.25
Expansion ratio	ϵ_{exp}	-	1.48

In general, the segmented setup allows for a high flexibility, meaning that the segments could easily be

exchanged with ones with e.g. different porous materials or enhanced measurement techniques.

2.2.2. Material Choice and Characterization

For the porous CMC liners, two different high temperature ceramic matrix composite materials are used. The four cylindrical liner segments are made up by the novel permeable CMC material OCTRA, which was developed at the DLR Institute of Structures and Design with the goal to obtain CMC materials with different porosities[12]. This allows for permeabilities adaptable to the requirements by the specific application. OCTRA40 is based on the LSI-C/C-SiC ceramics developed at DLR, which are modified with specifically designed porosities to allow a controlled permeability by design. For these materials, a defined portion of the carbon fibres within the baseline composite material was replaced with thermally non-stable aramid fibres. The fibres are degrading in the pyrolysis process step during manufacturing, leading to defined cavities inside the material. This allows for adjustable porosities in a range between 1% and 30% for the OCTRA material. However, due to this porosity insertion, the material is only permeable parallel to fibre direction, and impermeable orthogonally to the fibre plies. The material variant used in the upcoming study is OCTRA40, which is obtained using an aramid fibre ratio of approximately 40% in the first step, leading to a final open porosity of approximately 30%[12].

The nozzle segment is made up of the carbon fibre reinforced carbon (C/C), which was already extensively used for transpiration cooling experiments, e.g. in [4, 5, 6]. The material choice was made due to the relatively good machinability of the C/C material. For further details on the manufacturing process, the author refers to Heidenreich [13]. Due to the anisotropy of the material, the fibre plies were oriented orthogonally to the direction to the main flow, allowing high permeabilities in direction of the coolant flow. For a detailed description on the throughflow distribution of C/C in dependency on fibre direction, the author refers to Dittert et al.[14].

For characterizing the thermal response of the OCTRA and C/C samples, the specific heat capacity c_p and the thermal conductivity k had to be determined. As these parameters are significantly temperature dependent, the characterization was done in a temperature range between 20°C and 500°C. The specific heat capacity was determined using a differential scanning calorimeter HotDisk3500. The thermal conductivity was derived from the thermal diffusivity a via the relationship

$$a = \frac{k}{\rho \cdot c_p}, \tag{1}$$

with ρ being the density, which was determined as $\rho_{C/C}$= 1.39 g/cm^3 for C/C and $\rho_{OCTRA40}$= 2.05 g/cm^3 for OCTRA40. The thermal diffusivity was measured using a laser flash method. The resulting temper-

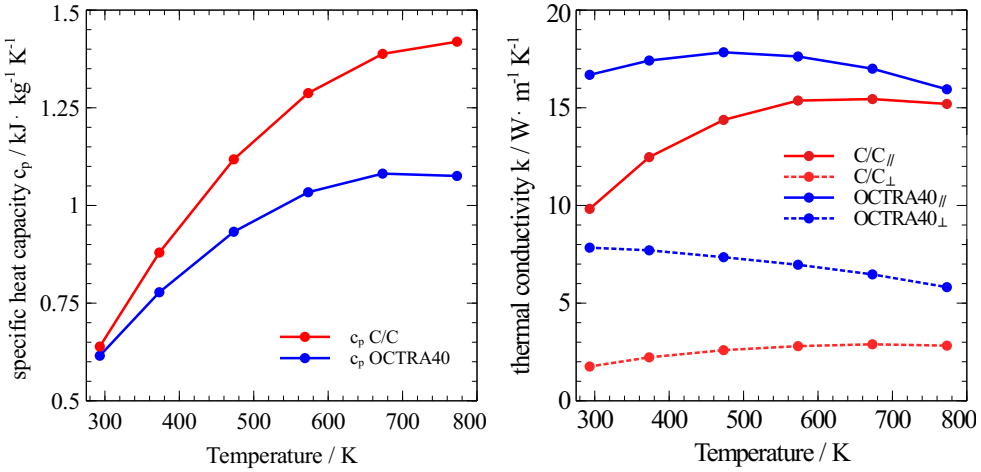

Fig 6. Measurement data of heat capacity c_p (left) and the thermal conductivity k (right).

ature dependent values of c_p and k are given in Figure 6. Due to the anisotropy of the CMC materials, k is given parallel to the fibre ply direction ($\parallel$) and orthogonal to the fibre ply direction ($\perp$).

The pressure loss of a fluid which is perfusing a porous medium can be described by the Darcy-Forchheimer equation which is formulated by Innocentini et al. [15] as

$$\frac{P_i^2 - P_o^2}{2P_oL} = \left(\frac{\mu}{K_D}\right)u_D + \left(\frac{\rho}{K_F}\right)u_D^2 \tag{2}$$

with the Darcy and Forchheimer coefficients K_D and K_F as the material specific permeation properties. The superficial Darcy velocity u_D can be derived from the coolant mass flow rate via the continuity equation

$$u_D = \frac{\dot{m}_{cg}}{\rho A_{cg}}. \tag{3}$$

The coefficients K_D and K_F were determined at the AORTA (Advanced Outflow Research Facility for Transpiration Application) test bench at the DLR Institute of Structures and Design [16]. Steady state pressure measurements were conducted using different mass flow rates of nitrogen at ambient temperature to obtain the pressure loss-mass flow curve. K_D and K_F were obtained in fitting Eq. 2 to the experimentally obtained curve, using a "least squares" algorithm. The uncertainties are determined using a Monte-Carlo method with a sample size of 200 000. The resulting Darcy and Forchheimer coefficients determined for each sample with their respective uncertainties are given in Table 3. For the nozzle segment, it has to be noted that the length used for the evaluation was the average wall thickness, hence, the measured permeability value is not representative for the C/C material.

Table 3. Permeability data of the investigated segments

Sample Order	**First (S1)**	**Second (S2)**	**Third (S3)**	**Fourth (S4)**	**Fifth (S5)**
Sample Geometry	Cylindrical	Cylindrical	Cylindrical	Cylindrical	Nozzle
Sample Material	OCTRA40	OCTRA40	OCTRA40	OCTRA40	C/C
K_D / m^2	$2.17E-12$	$1.82E-12$	$1.42E-12$	$1.57E-12$	$3.71E-13$
$\pm$ / m^2	$3.44E-13$	$2.313E-13$	$1.41E-13$	$2.09E-13$	$3.15E-14$
K_F / m	$1.50E-07$	$1.35E-07$	$1.483E-07$	$1.182E-07$	$4.22E-08$
$\pm$ / m	$2.68E-08$	$2.19E-08$	$2.66E-08$	$1.97E-08$	$1.013E-08$

2.3. Definition of Experimental Parameters

In the following, the respective experimental parameters of the hot gas and coolant flow are described. All measurements are conducted as stationary measurements. The HTF facility is controlled with a fixed hot gas bulk temperature measured at the inlet of the test section, as well as a fixed inlet pressure p_{hg}. This results in a variation of the hot gas mass flow $\dot{m}_{hg}$ with different coolant mass flow rates, due to the total mass flow being limited by the choked flow condition of the sonic nozzle. The resulting bulk velocities u_{hg}, Mach numbers $M_{hg,in}$ and Reynolds numbers $Re_{D,hg}$ are calculated with

$$u_{hg,in} = \frac{\dot{m}_{hg}}{\rho_{hg} \cdot A_{hg}} \tag{4}$$

$$M = \frac{u_{hg}}{\sqrt{\kappa R T_{hg}}} \tag{5}$$

$$Re_{D,hg} = \frac{u_{hg,in} \cdot d_h}{\mu_{hg}} \tag{6}$$

with the hydraulical diameter d_h = d_{cyl}. The resulting measured and calculated hot gas conditions are

Table 4. Summary of hot gas conditions

Parameter	Symbol	Unit	Value
Temperature	T_{hg}	K	800
Inlet pressure	p_{hg}	bar	6
Mass flow rate	$\dot{m}_{hg}$	g·s^{-1}	$230 - 262$
Bulk Velocity Inlet	u_{hg}	m·s^{-1}	$124 - 142$
Bulk Mach number inlet	$M_{hg,in}$	-	$0.22 - 0.25$
Reynolds number	Re_{hg}	-	$100099 - 114025$
Bulk Mach number outlet	$M_{hg,out}$	-	1.86

summarized in Table 4.
The coolant flow can be described with the dimensionless blowing ratio

$$F = \frac{\dot{m}_{cg}/A_{cg}}{\dot{m}_{hg}/A_{hg}} = \frac{u_{cg} \cdot \rho_{cg}}{u_{hg} \cdot \rho_{hg}} \tag{7}$$

which is the parameter kept equal for all perfused segments. The blowing ratios are calculated with A_{hg} being the cross-sectional area of the cylindrical segment and A_{cg} the respective outlet areas of the porous segments.

Table 5. Summary of mass flow rates

Test case	F / %	$\dot{m}_{cg,1-4}$/g·s^{-1}	$\dot{m}_{cg,5}$/g·s^{-1}	$\dot{m}_{hg}$/g·s^{-1}
0	0	0	0	262
1	0.05	0.60	0.74	259
2	0.10	1.20	1.46	257
3	0.15	1.77	2.17	254
4	0.25	2.91	3.56	250
5	0.38	4.30	5.26	246
6	0.5	5.63	6.86	241
7	0.63	6.91	8.44	237
8	0.75	8.05	9.83	230

3. Results of experimental Study

In the following, the results of the transpiration cooling study are being presented, with the focus on the one hand laying on the surface temperature distribution over the porous specimen, as well as the temperature distribution inside the porous material.

3.1. Surface temperature distribution

The hot gas side surface temperature distribution temperature distribution for the transpiration cooling experiments over the whole sample arrangement is shown in Fig. 7.

In general, for the cylindrical section of the test specimen, the temperature distribution shows the expected temperature drop with rising distance to the begin of the test section. This is caused by the build up of a cooling film by the injected coolant upstream, hence effectively reducing the heat flux on the wall. The blowing ratio has an significant impact on the cooling effect, as it decreases the wall temperature significantly from 730 K for the reference case without blowing to 404 K at the fourth sample for $F = 0.75\%$. The temperature reduction by the transpiration cooling seems to be mainly influenced by the first sample S1, as, especially for $F > 0.25\%$, the sharpest decrease of temperature

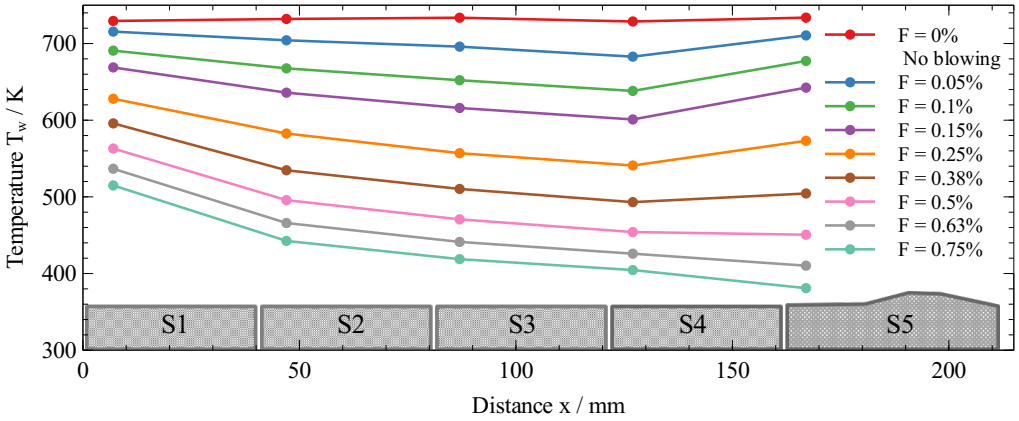

Fig 7. Surface Temperature Distribution with uniform blowing ratio

could be determined for this segment. Afterwards, for the downstream cylindrical segments, only a comparably moderate temperature reduction could be detected.

For the nozzle segment S5, an interesting blowing ratio dependent effect could be found. At a high blowing ratio of $F = 0.75\%$, the temperature decreases even sharper as for S2-S4. With lower blowing ratios, the relative temperature reduction decreases significantly, with no significant temperature reduction between S4 and S5 for $F = 0.5\%$. For $F < 0.5\%$, the wall temperature is higher than the upstream segment. This phenomenon could be caused by two concurrent effects. On one hand, the effectivity of the film cooling created by the upstream segments diminishes at low blowing ratio, allowing higher wall heat fluxes. On the other hand, an uneven distribution of the coolant mass flow inside the porous segment lead to locally low coolant effectivities. As the local coolant mass flow rate can be determined by Eq. 2 and Eq. 3, the main drivers are the hot gas side wall pressure and the local wall thickness. As the wall pressure decreases significantly in the divergent nozzle section due to the expansion, while having a similar wall thickness as in the convergent section, the coolant flows mainly into this section, as the highest pressure difference is existant there. This effect is further supported by the structure of the used porous material. As already mentioned in section 2.2.2, the OCTRA40 material was found to be practically impermeable in axial direction, the C/C material has also a significant permeability in axial direction, however with K_D and K_F being a order of magnitude lower than in radial direction [5]. This allows for cross flow in axial direction inside the porous nozzle segment due to axial pressure gradients. This has to be further investigated using computational fluid dynamics simulations, allowing detailed 2D simulations of the flow field inside of the porous material.
To further asses the effectiveness of transpiration cooling, the resulting surface temperatures are transferred into the dimensionless cooling efficiency

$$\Theta = \frac{T_{w,0} - T_w}{T_{w,0} - T_c} \tag{8}$$

which was introduced by Langener [4]. The determined cooling efficiencies plotted over the running length are shown in Fig. 8 In general, the high effectiveness of transpiration cooling could be shown, with Θ = 0.82 for F = 0.75%. For each investigated blowing ratio, Θ increases linearly over the running length for the cylindrical section. This suggests, that for the modeling of the accumulation of the transpiration cooling and the cooling film by the upstream samples, a linear superposition approach could be applied. The dependency of the cooling efficiency on the blowing ratio is illustrated for each sample position in Fig. 9. It can clearly be seen for S1-S4, that difference between S1 and S2 is the highest for every blowing ratio, with decreasing differences in cooling efficiency between S2-S4. This indicates that the temperature reduction created by the first sample is dominant. One could conclude from that for keeping a constant wall temperature, the coolant mass flow has to be controlled in a manner, that in the beginning of the cooled section, comparably high mass flow rates are required for

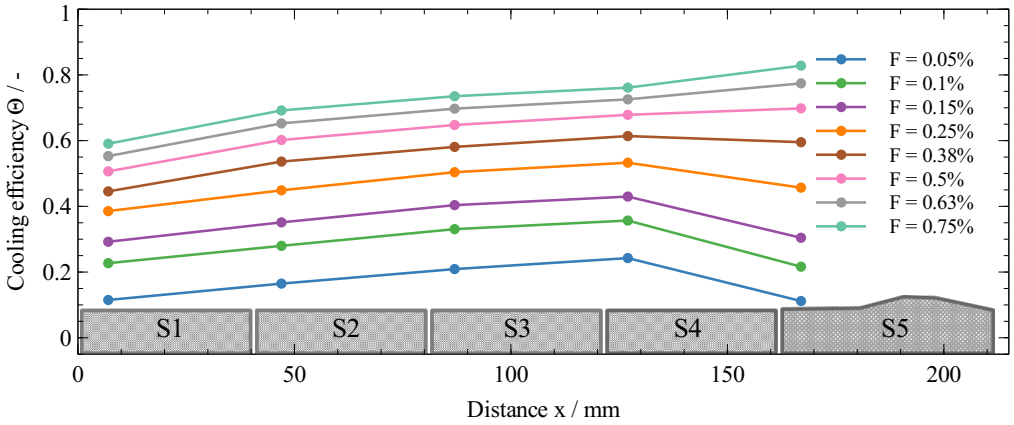

Fig 8. Cooling efficiency Θ with uniform blowing ratio

creating an initial high cooling effect, but that can be reduced significantly in downstream direction by utilizing the heat transfer reduction of the created cooling film.

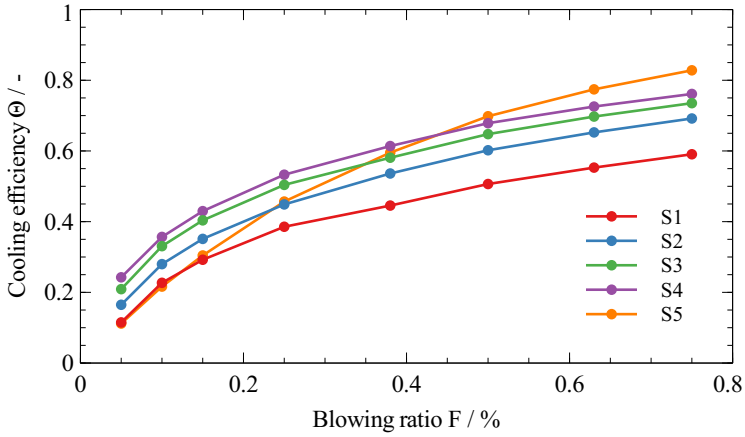

Fig 9. Cooling efficiency Θ in dependency of blowing ratio

3.2. Sample internal temperature distribution

To fully characterize the thermal response of the porous wall, the temperature profile inside the CMC liner has to be determined. However, measuring temperatures in a porous sample is difficult, as there is a solid and fluid phase in the porous medium, which can have different temperatures (local thermal non-equilibrium, LTNE). Due to the ceramic adhesive bonding, a well established contact to the bulk material can be assumed. Furthermore, the thermocouples may influence the through-flow of the coolant, hence manipulating the temperature distribution [4].

The measured temperature profiles inside the porous wall are given in Fig. 10. The diamond-shape symbols are denoting the coolant temperature in the plenum. The qualitative dependency on the blowing ratio can be seen most significantly at sample S1. With low blowing, at F = 0.05% , an almost linear decrease of temperature can be determined from the hot gas side surface (y = 10 mm) to the reservoir side surface (y = 0 mm). This can be related to the dominance of conduction effects over the internal heat transfer through the perfusion of the coolant. With increased blowing, the temperature tends to form a exponential shape, showing the effect of sample-internal heat transfer, as found by e.g. Langener et al. [4]. For samples further downstream, the temperature profile flattens significantly,

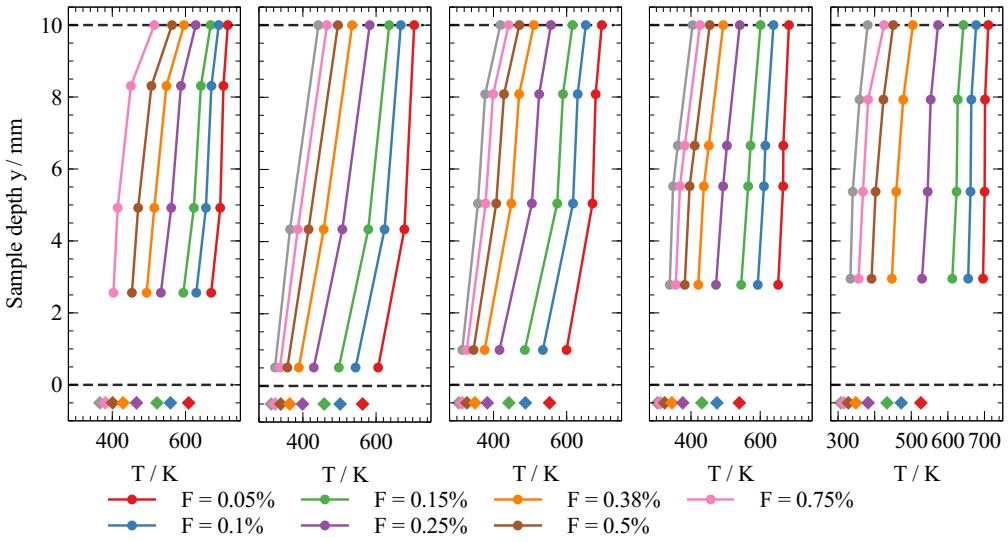

Fig 10. Sample Internal Temperature Distribution with uniform blowing ratio

caused by the decreased incoming heat transfer due to the film formation by the upstream samples. For the full assessment of the thermal situation inside the porous medium and subsequently the identification of LTNE, the volumetric heat transfer coefficient h_v for the porous materials has to be determined. This has to be investigated in further studies, as no data on h_v exists for OCTRA40, and only a rough estimation by Schweikert[5] for C/C exists.

4. Summary and Outlook

This paper presents the first results of a subscale combustion chamber with non-reactive flow conditions. The experiments were conducted with a hot air mainstream flow, with a bulk temperature of T_{hg} = 800 K and total pressure of p_0 = 6 bar. The five-segmented specimen was perfused with a blowing ratio uniform for each segment, of F = 0-0.75%. The experiments successfully demonstrated the high cooling efficiency of transpiration cooling in such a segmented setup, with Θ rising from 0.59 for the first segment up to 0.82 for the fifth segment. The almost linear increase of the cooling efficiency supports the hypothesis that a linear superposition approach could be used to model the accumulation of the transpiration cooling and film cooling from upstream samples. For the surface temperature distribution, it could be shown that the cooling effect provided by the first segment has an significant influence on the downstream samples. In a potential application where coolant mass flow has to be optimized, one approach could be in high blowing for the beginning of the cooled section and comparably low blowing for further downstream porous walls. The temperature rise for low blowing ratios in the nozzle segment could be explained by strong pressure gradients in the expansion section of the nozzle, diverting most of the coolant in this part. For the bulk temperature inside the porous liner segments, the influence of the decreasing wall heat flux with rising blowing ratio and distance to the first segment could be shown, as the temperature profile flattens significantly especially for high blowing ratios.

In future studies, analytical models for predicting the wall temperature have to be developed. This comprises both the effects through transpiration cooling, through the film cooling by the orthogonal blowing by the upstream transpiration cooling, as well as the superposition of both effects. Furthermore, the numerical tools for the analysis of transpiration cooling which were validated under moderate thermal conditions as described in Munk et al. [17] have to be tested under elevated thermal loads. For the transfer to design tools for combustion chambers, these analytical and numerical methods have to be fully qualified under realistic combustion chamber conditions, considering reactive flow, transient flow and thermal conditions as well as foreign gas transpiration. Here, the segmented test specimen was to be designed to be also tested under these conditions if attached to a suitable test rig.

5. Acknowledgements

The authors want to thank Fabian Siegler for the mechanical design of the transpiration cooling specimen.

Financial support has been provided by the German Research Foundation (Deutsche Forschungsgemeinschaft – DFG) in the framework of the Sonderforschungsbereich Transregio 40

References

[1] Suslov, D. ; Arnold, R. ; Haidn, O.: Investigation of Two Dimensional Thermal Loads in the Region Near the Injector Head of a High Pressure Subscale Combustion Chamber. In: *47th AIAA Aerospace Sciences Meeting including The New Horizons Forum and Aerospace Exposition* (2009)

[2] Eckert, E.R.G. ; Livingood, J.N.B.: Comparison of Effectiveness of Convection-, Transpiration-, and Film-cooling Methods with Air as Coolant / National Advisory Commitee for Aeronautics. 1953 (3010). – Technical Note

[3] Tully, L. R. ; Omar, A. ; Chung, J. N. ; Carroll, B. F. ; Tucker, P. K.: Fluid Flow and Heat Transfer in a Liquid Rocket Fuel Injector. In: *41th Joint Propulsion Conference* (2005), July

[4] Langener, T. ; von Wolfersdorf, J. ; Selzer, M. ; Hald, H.: Experimental investigation of transpiration cooling applied to C/C material. In: *International Journal of Thermal Sciences* 54 (2005), S. 70–81

[5] Schweikert, Sven: *Ein Beitrag zur Beschreibung der Ein Beitrag zur Transpirationskühlung an keramischen Verbundwerkstoffen*. Stuttgart, University of Stuttgart, PhD-Thesis, 2019

[6] Schwab, Andreas ; Peichl, Jonas ; Selzer, Markus ; Böhrk, Hannah ; von Wolfersdorf, Jens: Experimental Boundary Layer Investigation of a Stacked Transpiration Cooling Setup with Uniform Blowing Ratio. In: *HiSST: 2nd International Conference on High-Speed Vehicle Science*, 2020

[7] Peichl, J. ; Schwab, A. ; Selzer, M. ; Böhrk, H. ; von Wolfersdorf, J.: Innovative Cooling for Rocket Combustion Chambers. In: al, N.A. A. (Hrsg.): *Future Space-Transport-System Components under High Thermal and Mechanical Loads* Bd. 146. Cham : Springer Nature, 2021

[8] Ortelt, M. ; Hald, H. ; Herbertz, A. ; Müller, I.: Advanced Design Concepts for Ceramic Thrust Chamber Components of Rocket Engines. In: *5th European Conference for Aeronautics and Space Sciences* (2013)

[9] Förster, F. J. ; Drøske, N. C. ; Bühler, M. N. ; von Wolfersdorf, J. ; Weigand, B.: Analysis of flame characteristics in a scramjet combustor with staged fuel injection using common path focusing schlieren and flame visualization. In: *Combustion and Flame* 168 (2016), S. 204–216

[10] Hald, H. ; Ortelt, M. ; Fischer, I. ; Greuel, D. ; Haidn, O.: Effusion cooled CMC rocket combustion chamber. In: *AIAA/CIRA 13th International Space Planes and Hypersonics Systems and Technologies Conference* (2005)

[11] Dexter, C. E. ; Fisher, M. F. ; Hulka, J.R. ; Denisov, K. P. ; Shibanov, A. A. ; Agarkov, A. F.: Scaling Techniques for Design, Development, and Test. In: al., M. H. (Hrsg.): *Liquid Rocket Thrust Chambers: Aspects of Modeling, Analysis, and Design*. American Institute for Aeronautics and Astronautics, 2000

[12] Dittert, C. ; Kütemeyer, M.: OCTRA - Optimized Ceramic for Hypersonic Application with Transpiration . In: al., M. S. (Hrsg.): *Advances in High Temperature Ceramic Matrix Composites and Materials for Sustainable Development* Bd. 263. Hoboken : John Wiley & Sons, 2017

[13] Heidenreich, B.: Manufacture and Applications of C/C-SiC and C/SiC Composites. In: *Processing and Properties of Advanced Ceramics and Composites IV*

[14] Dittert, C. ; Selzer, M. ; Böhrk, H.: Flowfield and pressure decay analysis of porous cones. In: *AIAA Journal* 55 (2017), Nr. 3, S. 874–882

[15] Innocentini, M.D.M. ; Jr., A.C. R. ; Nascimento, L.A. ; Pandolfelli, V.C.: The pressure–decay technique for air permeability evaluation of dense refractory ceramics. In: *Cement and Concrete Research* 34 (2004), S. 293–298

[16] Selzer, Markus ; Schweikert, Sven ; Hald, Hermann ; von Wolfersdorf, Jens: Throughflow characteristics of C/C. In: *Sonderforschungsbereich/Transregio 40 Annual Report 2014*. Garching, 2014

[17] Munk, D. ; Selzer, M. ; Böhrk, H. ; Schweikert, S. ; Vio, G.: Numerical Modeling of Transpiration-Cooled Turbulent Channel Flow with Comparisons to Experimental Data. In: *Journal of Thermophysics and Heat Transfer* 32 (2018), July, Nr. 3, S. 713–735